Manuscript details

Manuscript number	HE_2015_1016
Title	Assessment of hydrogen storage in activated carbons produced from hydrothermally treated organic materials
Article type	Full length article
Abstract	12 activated carbons (ACs) were prepared by KOH activation using hydrochars as precursors. These hydrochars were prepared by hydrothermal carbonisation (HTC) of sucrose solutions at concentrations ranging from 0.2 to 1.6 mol L-1. The KOH to hydrochar weight ratio (W) was varied from 1 to 5, and the activation temperature was set to 1023K. ACs texture was assessed by nitrogen and carbon dioxide adsorption at 77 and 273 K, respectively; pore size distribution was calculated by using both isotherms and the SAIEUS© software. ACs with surface areas between 790 and 2240 m2 g-1 were obtained. Hydrogen excess adsorption was determined at 298K and pressures up to 10 MPa in a volumetric device, and the isosteric heat of adsorption (Qst) was calculated for four ACs, using hydrogen isotherms obtained at 278, 298 and 308K. Potassium intercalation between graphitic planes was assumed to account for the high Qst values, 7-8 kJ mol-1. Hydrogen uptake at 2 MPa was compared with hydrogen adsorption data of 38 other ACs reported in the open literature.

	Hydrogen adsorption fundamentally depends on micropore volume and preliminary HTC did not enhance hydrogen storage although it could be a good strategy for doping carbon with heteroelements.
Keywords	hydrogen storage; adsorption; hydrothermal carbonisation; KOH activation; microporous activated carbons.
Manuscript category	Hydrides / Storage / Capacitors
Corresponding Author	Vanessa Fierro
Order of Authors	Sébastien Schaefer, Vanessa Fierro, Maria Teresa Izquierdo, Alain Celzard
Suggested reviewers	Juana Gervasoni, Edilso Reguera, Fabian Suarez-Garcia

Submission files included in this PDF

File Type	File Name
Cover Letter	H2_HTC_IJHE_letter_revisd version.doc
Response to reviewers	answers to reviewers_final.docx
Highlights	schaefer_HTC_highlights.docx
Manuscript	HTC_H2_vf_manuscript_HE_revised_final.docx
Figure	schaefer_fig1.docx
Figure	schaefer_fig2.docx
Figure	schaefer_fig3.docx
Figure	schaefer_fig4.docx
Figure	schaefer_fig5.docx

Figure	schaefer_fig6.docx
Figure	schaefer_fig7.docx
Figure	schaefer_fig8.docx
e-Component	Supplementary material.docx

To view all the submission files, including those not included in the PDF, click on the manuscript title on your EVISE Homepage, then click 'Download zip file'.

Assessment of hydrogen storage in activated carbons produced from hydrothermally treated organic materials

S. Schaefer[a,b], V. Fierro[*a,b], M.T Izquierdo[c], A Celzard[a,b]

[a] Université de Lorraine, ENSTIB, 27 rue Philippe Séguin, CS 60036, 88026 Épinal cedex, France

[b] Institut Jean Lamour, UMR CNRS 7198, ENSTIB, 27 rue Philippe Séguin, CS 60036, 88026 Épinal cedex, France

[c] Instituto de Carboquímica,: Miguel Luesma Castán, 4. Zaragoza. E-50018, España

[*] Corresponding author. Tel: + 33 329 29 61 77. E-mail: Vanessa.Fierro@univ-lorraine.fr (V. Fierro)

Abstract

12 activated carbons (ACs) were prepared by KOH activation using hydrochars as precursors. These hydrochars were prepared by hydrothermal carbonisation (HTC) of sucrose solutions at concentrations ranging from 0.2 to 1.6 mol L^{-1}. The KOH to hydrochar weight ratio (*W*) was varied from 1 to 5, and the activation temperature was set to 1023K. ACs texture was assessed by nitrogen and carbon dioxide adsorption at 77 and 273 K, respectively; pore size distribution was calculated by using both isotherms and the SAIEUS© software. ACs with surface areas between 790 and 2240 m^2 g^{-1} were obtained. Hydrogen excess adsorption was determined at 298K and pressures up to 10 MPa in a volumetric device, and the isosteric heat of adsorption (Q_{st}) was calculated for four ACs, using hydrogen isotherms obtained at 278, 298 and 308K. Potassium intercalation between graphitic planes was assumed to account for the high Q_{st} values, 7-8 kJ mol^{-1}. Hydrogen uptake at 2 MPa was compared with hydrogen adsorption data of 38 other ACs reported in the open literature. Hydrogen adsorption fundamentally depends on micropore volume and preliminary HTC did not enhance hydrogen storage although it could be a good strategy for doping carbon with heteroelements.

hydrogen storage; adsorption; hydrothermal carbonisation; KOH activation; microporous activated carbons.

1. Introduction

Hydrogen is an energy vector which should be extensively used in the future. Storing energy by generating hydrogen during electricity production peaks might be a complementary alternative to the establishment of regulated energy networks like Smartgrids [1]. Several pilots plants, such as the MYRTE demonstrator in France, are converting solar energy into electricity, then into hydrogen, and they have already proved their efficiency [2].

Hydrogen storage at high pressure or in liquid state is controversial due to security issues that also imply social acceptability [3, 4]. Hydrogen adsorption on a solid surface allows reducing the storage pressure but requires low temperatures to enhance adsorption capacity. However, hydrogen storage at moderate pressures, lower than 4MPa, and at room temperature remains a challenge. The theoretical upper limit for hydrogen storage in carbon materials is around 6.9 wt.% at 77K [5], and such value was already experimentally attained with some activated carbons [6-8]. This value is higher than the 5.5 wt% recommended by the DOE for automotive applications in 2017.

Nevertheless, not only the weight of the storage material but that of the entire system has to be taken into account. Therefore, 5.5 w% of the adsorbent weight is not enough. Moreover, the DOE recommends meeting such capacities in the 233 – 358K temperature range, whereas the aforementioned values were measured at 77K [9]. Still, lower capacities can be accepted for stationary applications, for which volume and weight are not limiting factors. As a consequence, the search for carbon materials able to store hydrogen at room temperature remains a hot topic nowadays. Activated carbons produced by KOH activation after a previous hydrothermal carbonisation (HTC) step of a variety of organic materials (saccharides, biomass or furfural) exhibited high hydrogen uptakes at 77K, up to 6.4 wt.% and high isosteric heat of adsorption, between 6 and 8.5 kJ/mol [10].

Researches on HTC and on other treatments in pressurised hot water started at the beginning of the 20th century [11-13]. HTC is the thermal treatment of a carbon precursor, whether natural or not, in water under moderate temperature and self-generated pressure in an autoclave. The latter induces both reaction and nucleation processes [14]. HTC occurs typically in the range 403-523K, and the recovered materials are called hydrothermal carbons or hydrochars [15]. Most of the times, when a solution is submitted to HTC hydrochars present a microsphere-like morphology [16-18] that sometimes remains after KOH activation [16-18]. Many organic precursors were treated by HTC to produce carbon materials, e.g. starch, sawdust, glucose, tannins, chitosan or glucosamine [10, 16, 19, 20]. When carbohydrates are involved, HTC proceeds by hydrolysis and intramolecular dehydration and polycondensation of the hydrolysis products [11]. These reactions lead to the formation of amphiphilic macromolecules forming micelles, which nucleate by dehydration and grow via a diffusion process [14]. Increasing the initial concentration of the carbonaceous precursor in the solution induces the increase of the average microsphere diameter [14, 16].

HTC is also an interesting method to produce carbons doped with heteroatoms such as nitrogen. Thus, nitrogen-rich carbonaceous materials were synthesised from tannin submitted to HTC in concentrated ammonia [21]. These materials can be carbonised and physically or chemically activated to obtain carbon materials with high and tuneable porosity for specific applications [18, 21, 22]. Indeed, according to several authors, these materials have a high potential for gas sorption and especially for carbon dioxide or hydrogen adsorption [23, 24]. The objective of the present study was to provide unquestionable proofs or rebuttals of the beneficial effect of a hydrothermal pre-treatment to synthetize activated carbons for hydrogen storage. For this purpose, hydrochars were produced by submitting sucrose solutions to HTC and these hydrochars were further activated with KOH. We studied the effect of both the initial sucrose concentration and the ratio KOH/hydrochar on the textural properties of the

resultant activated carbons (ACs), and hence on their hydrogen storage performances. Our results were compared with those reported in the open literature.

2. Experimental

2.1. Preparation of hydrochars

Sucrose of purity 99%, supplied by Sigma Aldrich®, was used as precursor. Sucrose solutions were prepared at different concentrations in bi-distilled water, namely: 0.2, 0.4, 0.8 and 1.6 mol L^{-1}.

HTC reactions were carried in 125 cm^3-capacity Teflon-lined autoclaves supplied by Parr Instrument Company® under reference "*Large Capacity Acid Digestion Vessel – Model 4748*". To avoid contamination of the Teflon pot during the synthesis, the sucrose solution (30 cm^3) was poured into a glass insert fitting the dimensions of the Teflon pot. Doing this, the available inner volume of the autoclave decreased to 100 cm^3. The oven was preheated at 453K and once the temperature was constant, the autoclaves were introduced in the oven and left for 24h. After thermal treatment, the autoclaves were cooled and the solutions were filtrated to recover the solid fraction, i.e. the hydrochar, which was dried in a vacuum oven at 353K and 15 kPa overnight.

2.2. Activation

Hydrochars were carbonised and activated in a single step-process using potassium hydroxide (KOH) as activating agent. KOH lentils and hydrochars were ground together in a weight ratio KOH to hydrochar (*W*) ranging from 1 to 5, and the resultant blends were put in a nickel crucible placed inside the stainless steel reactor of a tubular oven. The tube length was 1.20 m and its inner diameter was 0.12 m. A heating rate of 3 K min^{-1} was applied up to the

final temperature, 1023 K, which was maintained for 1h. The oven was continuously flushed by a 70 cm^3 min^{-1} nitrogen flow during the whole activation process: heating, plateau and cooling.

After activation, the obtained activated carbons (ACs) were washed with a 0.1 mol L^{-1} solution of hydrochloric acid, then with bi-distilled water, and finally were thoroughly washed in a Soxhlet extractor with water for 3 days. For that purpose, the ACs were put in dry cellulose cartridges of know weights before putting them in the Soxhlet. Finally, the cartridges were dried in a ventilated oven at 378K and weighed for calculating the AC yield (Y_{AC}) determined as:

$$Y_{AC} = \frac{activated\ carbon\ (g)}{precursor\ (g)}\ x\ 100$$

where precursor stands for hydrochar when HTC was used or, sucrose or prysolysed sucrose as we will see afterwards.

The samples were labelled AcHTC_M_W, where "Ac" means that the material was activated, "HTC" has the same meaning as before, "M" (molarity) stands for the concentration of the initial solution, and "W" is the activation ratio. Labels comprising neither "Ac" nor *W* values correspond to hydrochars, i.e. to non-activated materials. For instance HTC_0.4 was the hydrochar obtained after HTC of a 0.4 mol L^{-1} sucrose solution.

Two complete sets of samples were prepared. The first one comprises 5 samples prepared by HTC of a 0.4 mol L^{-1} sucrose solution, whose resultant hydrochars were activated with KOH according to different ratios *W* of 1, 2, 3, 4 and 5. The second set comprises 4 samples prepared by HTC of sucrose solutions with different initial concentrations of 0.2, 0.4, 0.8 and 1.6 mol L^{-1}, whose resultant hydrochars were activated with KOH according to $W = 4$.

For the sake of comparison, 6 other samples were prepared by two methods: (i) by direct KOH activation of sucrose (*1step* sample set) at 1023K and (ii) by dry pyrolysis of sucrose at 1023K followed by KOH activation at the same temperature (*2steps* sample set). For these two precursors, sucrose and pyrolyzed sucrose, we used and equivalent activating ratio, Weq, in order to maintain constant the ratio KOH/C and it was calculated as:

$$W_{eq} = \frac{C_{precursor}}{C_{HTC}} * W$$

where W is activation ratio of hydrochars and is equal to 1, 3, or 5. $C_{precursor}$ and C_{HTC} are the carbon weight percentage in the precursors (i.e sucrose or pyrolized sucrose) and hydrochar respectively as obtained by elemental analysis. Thus, *1step* sample set was obtained after activating sucrose with KOH using *Weq* = 0.63, 1.89 and 3.15. *2steps* sample set was prepared after activating pyrolized sucrose with KOH using *Weq* = 1.34, 4.27 and 6.75. These samples were named 1step_*Weq* and 2steps_*Weq*.

The total yield (Y_T) was calculated as the product $Y_{HTC} \times Y_{AC}$, when using HTC as pretreatment, and as the product $Y_{PYR} \times Y_{AC}$, when using pyrolysis as pretreatment. Y_{PYR} stands for the pyrolysis yield. For direct activation of sucrose, Y_T is equal to Y_{ACT} as there is not any pretreatment.

2.2 Characterisation

2.2.1 Textural properties

The textural characterisation of the ACs was performed using an automatic adsorption apparatus ASAP 2020 from Micromeritics®. The ACs samples were degassed under vacuum at 523K until the pressure stabilised around 0.2 to 0.4 mPa for more than 24h, and weighed. Further degassing was carried out at the measuring port for 6h at least. Cool and warm volumes were determined after nitrogen or carbon dioxide adsorption to avoid helium

entrapment in the narrowest pores. The analyses were carried out with nitrogen and carbon dioxide adsorption at 77 and 273 K, respectively. All the data were treated using the Microactive software from Micromeritics®.

The BET apparent surface area, S_{BET}, was obtained using the BET equation in the appropriate range of relative pressures. Micropore volumes and micropore surface areas were obtained using the Dubinin-Raduskevich (DR) equation. The average micropore diameter, L_0, was calculated using 2D-NLDFT model from Jagiello et al. [25, 26]. The pore size distributions (PSDs) were obtained using non-local density functional theory (NLDFT) from the Solution of Adsorption Integral Equation Using Splines (SAIEUS®) program. SAIEUS® has the advantage of combining both CO_2 and N_2 adsorption data to get more accurate PSDs. Moreover, it allows to fit the PSDs with a spline model and to avoid the usual singularities of the classical DFT model. The smoothing parameter λ, with initial values close to 4.5, was set constant and equal to 4.5 for all the samples in order to allow comparison between the different PSDs.

The skeletal density of the solids was obtained by helium pycnometry using an AccuPyc II 1340 apparatus from Micromeritics. The samples were previously degassed at 373K under vacuum. The analysis was performed at 303K in order to avoid He adsorption.

2.2.2 Elemental Analysis

Ultimate analyses of samples were carried out in a CHONS elemental analyser (Vario El Cube, Elementar, Germany) to determine first carbon, hydrogen, nitrogen and sulphur contents by combustion of the samples in a stream of pure O_2. Oxygen was analysed with the same equipment in a second step, using a different procedure.

2.2.3 Hydrogen adsorption

Hydrogen adsorption experiments were carried out at 298K using a HPVAII automatic adsorption apparatus from Micromeritics-Particulate-Systems. A 10 cm^3 chamber was used for an average sample amount of 1g. The temperature control was set to 293K for the cold volume measurement and then was changed to 298K for the warm volume measurement and experiment. The pressure steps for adsorption were 0.05, 0.15, 0.3, 0.6, 0.8, 1, 1.5, 2, 3, 4, 6, 7, 8, 9 and 10 MPa. The pressure steps for desorption were 8.5, 7.5, 6.5, 5.5, 4.5, 3.5, 2.5 and 2 MPa. The contribution of the empty cell was systematically measured and subtracted to all data in order to improve the accuracy.

The isosteric heat of adsorption was calculated using the isosteric method from the Microactive software from Micromeritics, based on the Clausius-Clapeyron equation:

$$-\frac{Q_{st}}{R} = \frac{\partial \ln(P)}{\partial(1/T)}$$

where R (8.314 J mol^{-1} K^{-1}) is the gas constant, P (Pa) is the absolute pressure and T (K) is the temperature. The calculation of Q_{st} was performed for four solids of the series AcHTCs_0.4_W (W = 1, 2, 3 and 4). Q_{st} was calculated using three isotherms obtained at 288, 298 and 308K. An average Q_{st} value was calculated over the whole range of hydrogen uptakes, i.e. over the whole range of pore diameters.

3. Results and discussion

3.1 Solids characterisation

3.1.1Morphology

Fig. S1 of the Supplementary material shows the typical spherical morphology of sucrose-derived hydrochars. The diameter of the carbon spheres increased with the sucrose concentration, in agreement with other findings [14, 16]. This phenomenon is due to a mechanism controlled by diffusion, making the concentration be the parameter leading the particle growth [14].

KOH activation destroyed most of the microspheres. Fig. 1 indeed presents the material HTC_0.4 before and after activation at $W = 4$ (AcHTC_0.4_4). Foam-like morphologies were observed, based on either wide (10 – 40µm) or much smaller cells (< 5µm). This foam-like morphology might be due to the gases produced by the various reactions occurring between organic matter and alkaline hydroxides, as already observed and reported for activated carbons derived from tannin-based hydrogels [27].

Some regions of spherical carbons similar to the ones reported by Romero-Anaya et al. [18] still remained. But unlike what the latter authors reported, who found that the spherical shape was mostly maintained at $1 \leq W \leq 3$, it was found here that such typical morphology almost disappeared after KOH activation in the same range of W. The amount of remaining microspheres decreased when W increased. Our results are well in agreement with Sevilla et al. [8] who found conchoidal cavities and smooth surfaces regardless of the hydrochar precursor.

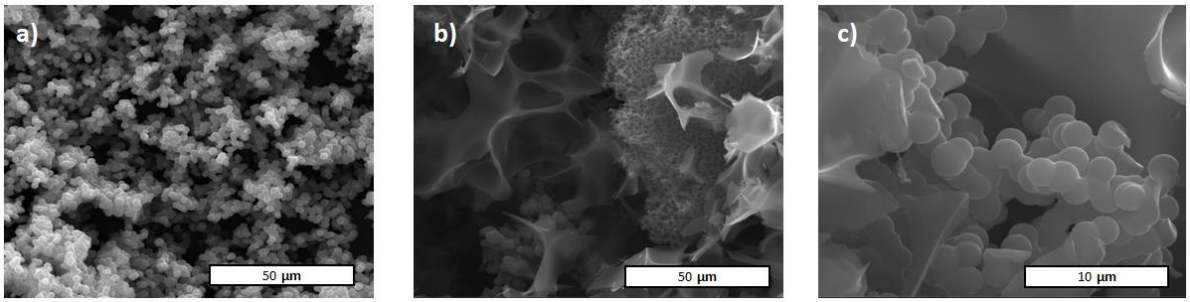

Fig. 1: SEM pictures of the HTC_0.4 hydrochar: (a) before (× 1000), and (b-c) after activation at $W = 4$ (× 1000 and × 5000, respectively).

3.1.2 Elemental analysis

Fig. 2 shows the data obtained by elemental analysis of hydrochars and ACs, plotted in the form of a Van Krevelen's diagram. Neither error bars nor box-plots were presented on this figure, as these statistical values were too small with regard to the used scale. Sucrose had H/C and O/C atomic ratios of 1.83 and 0.92, respectively.

Due to dehydration reactions, the hydrochars presented significantly lower H/C and O/C atomic ratios with respect to glucose. According to Sevilla et al. [11], the first step of HTC is the hydrolysis of sucrose, leading to the formation of glucose and fructose, which decompose into acids such as levulinic, acetic, lactic and formic acids. The protons released by these acids catalyse the degradation of sucrose. Dehydration and fragmentation of the as-obtained monosaccharides lead to formation of furfural-like compounds. Then, the decomposition of the latter produces aldehydes and ketones. Fructose and glucose subsequently polymerise while ketones and aldehydes react through aldol condensation [11]. H/C and O/C atomic ratios after HTC were very similar for all the hydrochars, irrespective to the initial concentration of the sucrose solutions submitted to HTC, as shown in the upper inset of Fig. 2. H/C and O/C atomic ratios were indeed found in narrow ranges: 0.82-0.87 and 0.33-0.34, respectively.

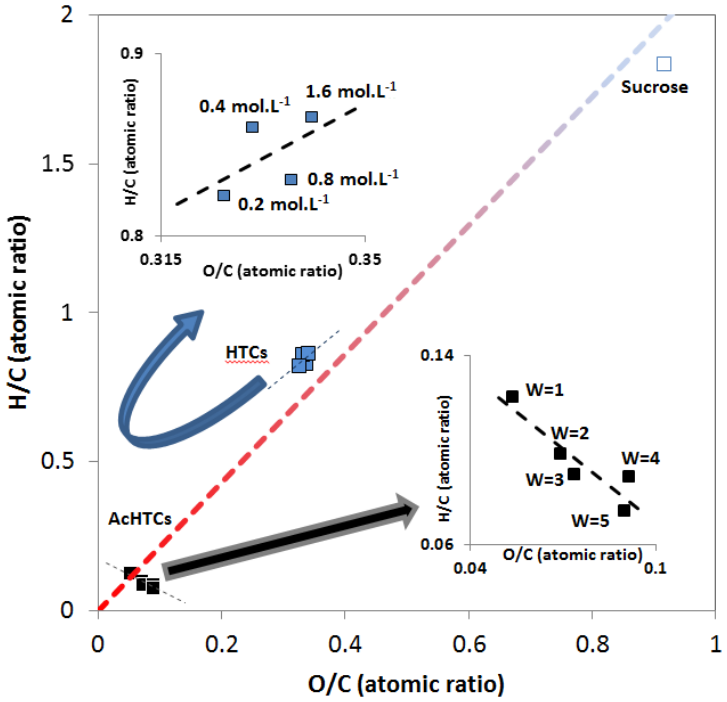

Fig. 2: Van Krevelen diagram of all the solids used or prepared in the present work. Upper and lower insets show the details for hydrochars before and after activation, respectively.

The lower inset of Fig. 2 gathers the atomic ratios of the activated hydrochars. H/C decreased whereas O/C increased when *W* increased, both ratios being also confined in a rather narrow ranges of values. The H/C and O/C atomic ratios, averaged for each *W*, indeed varied from 0.07 to 0.12 and from 0.05 to 0.09, respectively. These values were much lower than those of the hydrochars, due to both evolution of volatiles and oxygen release in the form of CO and CO_2 [28]. The increase of the O/C ratio with *W* is due to the carbon oxidation by CO_2 produced from K_2CO_3 decomposition, the latter being formed in situ. KOH activation has indeed been described as a combined chemical-physical activation [29].

3.1.3 Yields to hydrochar and activated carbon

Fig. 3a) shows the hydrochar yield (Y_{HTC}) as a function of the initial concentration of sucrose in the solution. The values of Y_{HTC} were 41, 44, 46, 49 wt.% for sucrose concentrations of 0.2, 0.4, 0.8 and 1.6 mol L^{-1}, respectively. The box-plots show the median

value, the first and third quartile (the body of the box is centred on the mean), and the maximum and minimum values of the measurements. According to the difference between maximum and minimum values, it can be asserted that Y_{HTC} significantly depend on sucrose concentration, at least for the two extreme values: 0.2 and 1.6 mol L^{-1}. The increase of Y_{HTC} with sucrose concentration is due to the corresponding increase of nucleation and growth rate, which mainly relies on concentration. These results are in good agreement with those found for glucose [22] and for tannin [16].

Fig. 3b) shows the activation yield (Y_{AC}) as a function of *W*. Y_{AC} values were found to be in a narrow range for any given *W*. *W* equal to 3, 4, and 5 produced activation yields in the ranges 26-31%, 21-26% and 15-19%, respectively. This is a usual trend for chemical activation based on KOH. Differences are within the range of the experimental error.

Fig. 3c) shows the total yield (Y_T) for the three types of ACs produced. For ACs prepared after HTC, Y_T decreased when *W* increased, with values ranging from 20.5 wt.% for $W = 1$ to 7.7 wt.% for $W = 5$, irrespective to the initial sucrose concentration. Dry pyrolysis of sucrose led to Y_T between 16.5 and 9.2 wt%, similar to those determined after HTC of sucrose. In contrast, direct activation of sucrose led to extremely small Y_T, between 6.0 and 1.4 wt%, making the process very unfavourable.

For practical applications, as important as the S_{BET} is the total carbon yield. Fig. 3d) shows the average values of the product $Y_T \times S_{BET,}$ already used as a performance criterion for the activation process [30], as a function of *W*. Concerning ACs prepared after HTC, the product $Y_T \times S_{BET}$ increased when increasing W, but between $W = 3$ and $W = 5$ differences were small, around 3%. For the 1step set of samples, direct activation of sucrose, the product $Y_T \times S_{BET}$ has the same behaviour than Y_T. This can be explained by an important decrease of Y_T and the similar S_{BET}, between 974 and 1016 m^2/g, when *W* increases. For the 2steps set of samples,

KOH activation after pyrolysis, the product $Y_T \times S_{BET}$ was higher than those for carbons produced by HTC before KOH activation and presented an optimum at W=3.

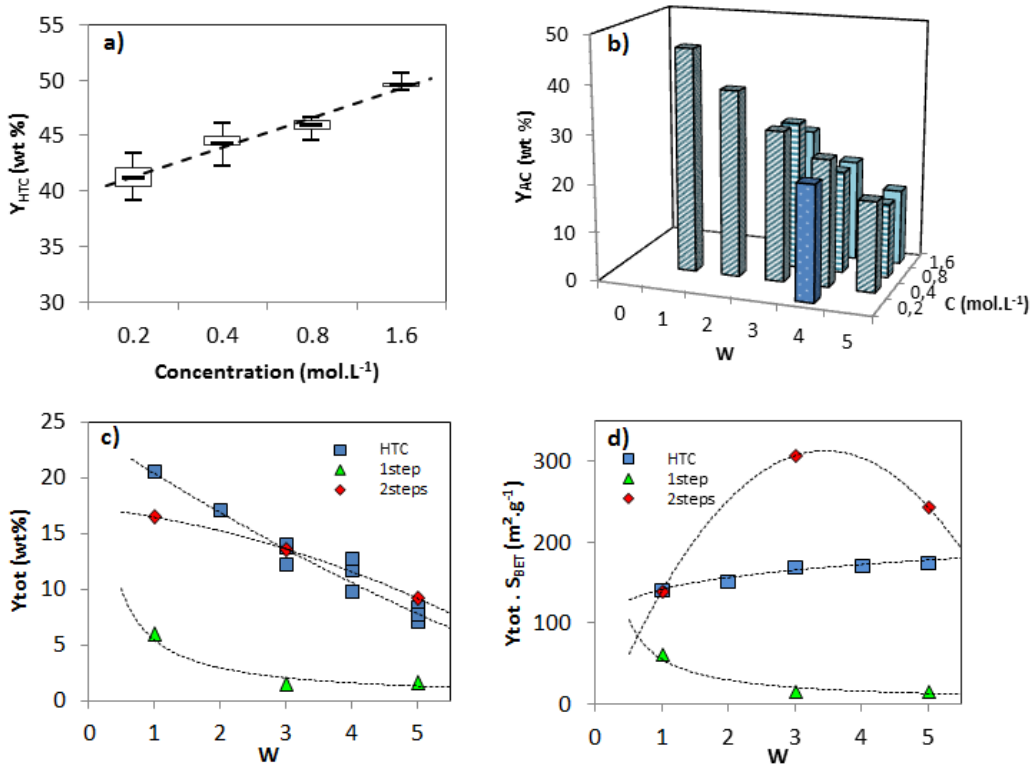

Fig. 3: Materials yield at different steps of the process: (a) after HTC of sucrose as a function of sucrose concentration; (b) after activation of hydrochars as a function of activation ratio and sucrose concentration; (c) Total yield and (d) surface yield from sucrose to activated carbons as a function of activation ratio (W) and on the process: ■ HTC+KOH activation, ▲ direct KOH activation (1 step) or ◆pyrolysis and KOH activation (2steps)

In order to explain the different behaviours upon KOH activation of pyrolysed sucrose, hydrothermally treated sucrose and pristine sucrose, we submitted these three precursors to pyrolysis in a thermogravimetric device and the evolved gases were analysed by mass spectrometry. Pyrolysed sucrose had a higher thermal stability than hydrochar and the later more than pristine sucrose when temperature increased (Fig. S2 of the Supplementary material). The maximum weight loss was also detected at different temperatures for each

precursor: 580, 670 and 880K for pristine sucrose, hydrochar and pyrolysed sucrose, respectively. In the temperature range 303-1173K, mass losses for pyrolysed sucrose, hydrochar and pristine sucrose were 12.48, 48.00 and 76.83 wt%, respectively. Pyrolysed sucrose had high carbon content (more than 90%) with lower emission of volatiles than HTC-sucrose and pristine sucrose. Fig. S3 of the Supplementary material shows the evolution of masses 28 (CO) and 44 (CO2). Pristine sucrose produced more CO_2 than hydrothermal sucrose and much more than pyrolysed sucrose. It appears than precursors containing more volatiles were more severely affected by KOH activation; the earlier volatile evolution would favour both the reaction of KOH with carbon at lower temperatures and a superactivation leading to a lower yield and surface area. The same effect was found in ACs from different rank coals; coals with a higher volatile content presented KOH-carbon reactions at lower temperatures [31]. Despite the fact that dry pyrolysis produced a higher $Y_T \times S_{BET}$ than HTC, HTC needs lower energy and no inert gas consumption, and therefore allows synthetizing doped carbon materials by a one-pot approach.

3.1.4 Textural characterization

Fig. 4a) presents the nitrogen adsorption isotherms of the AcHTC_0.4 series. All of them were type I, characteristic of microporous materials according to the IUPAC classification. For low *W*, the isotherms presented a large amount of adsorbed nitrogen at very low pressure as well as very narrow knees, which is typical of fundamentally ultramicroporous solids. Increasing *W* produced both the broadening of the knees, which indicates the development of wider micropores, and higher nitrogen uptakes in the whole range of relative pressures, indicating that pore volume increased in the whole porosity range. No hysteresis loops were observed for any of the AC studied.

Fig. 4b) shows the carbon dioxide adsorption isotherms of the same ACs as in Fig. 4a). Both figures showed the same trend, i.e. higher adsorbed volumes for higher *W*, thereby confirming the development of the porosity for the whole pore diameter range, including the very narrow porosity only accessible to CO_2.

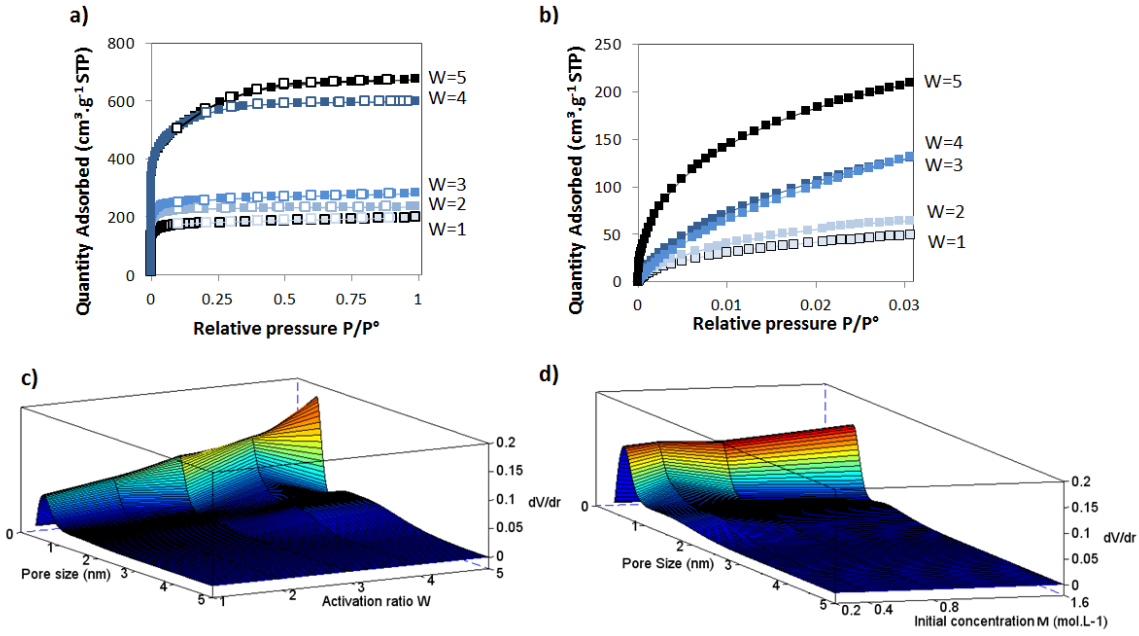

Fig. 4: Adsorption isotherms and pore size distributions of the AcHTC_0.4 series using: (a) N_2 and (b) CO_2 as probe molecules. Pores size distributions of ACs as a function of (c) activation ratio *W* (with M=0.4M) and of (d) concentration *M* (with W=4).

Fig. 4c) shows the PSDs obtained by application of the 2D-NLDFT model to the isotherms presented in Fig. 4a) and 4b). The activated carbons were essentially microporous, as 59 to 97% of their total volume was made of micropores. The PSDs were bimodal with a first peak around 0.50-0.65 nm and the second one at 1.25-2.00 nm, both in the micropore range. Indeed, the first peak maintained his position around 0.5 nm for all *W* values from 1 to 5, whereas a second appeared around 1.3 nm and moved progressively to 1.9 nm when *W* increased from 3 to 5. Maxima of the PSDs were reported in Tables S9 and S10 of the

Supplementary material. Fig. 4d) shows the effect of sucrose concentration, *M*, on the PSD at constant *W* = 4. No significant influence was found. Detailed data of textural properties can be found in Table S9 of the Supplementary material.

Fig. 5a) shows the effects of *W* and *M* on the micropore volume. Micropore volume was highly dependent on *W*, but not on *M* (see Fig. S4 of the Supplementary material). Fig. 5b) presents the correlation between volume and width of micropores. Increasing *W* produced a widening of the pores, as shown in Fig. 4c), but also an increase of the total micropore volume.

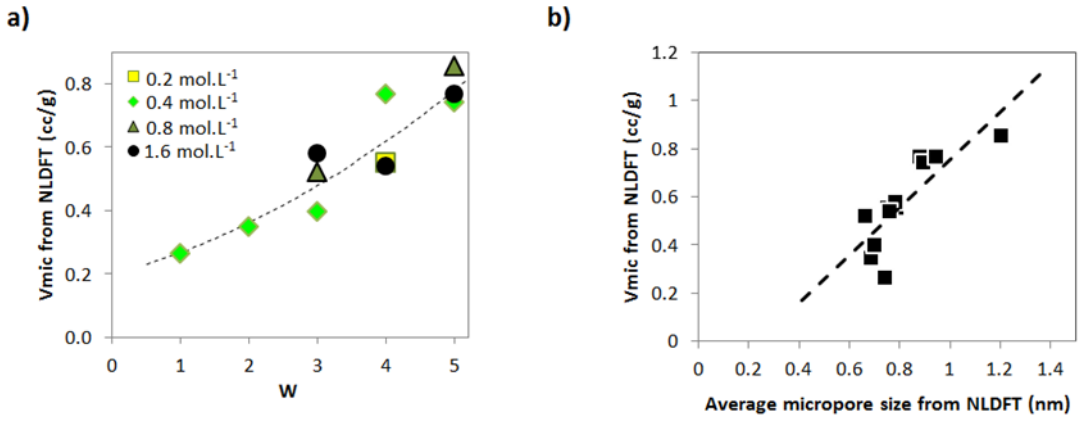

Fig. 5: a) Effect of *W* on the micropore volume of the AcHTC_0.4 series; b) Correlation between micropore volume (V_{mic}) and average micropore size (L_0).

The skeletal density of the ACs ranged from 1.93 to 2.35 g cm^{-3} (see Fig. S5 of the Supplementary material). The highest densities, higher than that of graphite, may be explained by the presence of potassium ions remaining intercalated in the carbon structure, despite the washing steps with hydrochloric acid and hot water [32, 33]. The latter assumption is in agreement with the fact that the highest densities were observed for the ACs prepared at the highest *W* ratios. Previous studies allowed us to obtain potassium content between 0.1 and 4 wt. % for KOH activated anthracites. Even, if a chemical analysis of these particular ACs was

not carried out, we can reasonably assume that potassium remained in the carbon based on the increasing density with W ratio.

3.1.5 Hydrogen adsorption

Fig. 6a) shows the hydrogen adsorption isotherms of 3 ACs: Ac_HTC_0.4_1, Ac_HTC_0.4_3 and Ac_HTC_0.4_5, presenting specific surfaces calculated with NLDFT ($S_{tot\ NLDFT}$) equal to 792, 1232 and 2242 $m^2\ g^{-1}$, respectively. The uptake increased with surface area for any fixed equilibrium pressure. Unlike hydrogen adsorption isotherms measured at 77K, isotherms at 298K did no present any maximum. This is a typical behaviour, as a maximum of hydrogen excess can only be found at temperatures lower than 200K [34, 35]. Hydrogen adsorption was fully reversible, and no hysteresis loop was observed. Hysteresis loop *in* hydrogen adsorption-desorption on ACs is indeed produced either by condensation in mesopores or by chemical adsorption, both being unlikely. As its critical temperature and pressure are 32.8 K and 1.28 MPa, respectively, hydrogen is indeed in the supercritical state or at least gaseous in the present experimental conditions [36], which makes condensation in mesopores highly improbable. Moreover, the solids do not contain any metal in a valence state that might induce chemisorption, related desorption delays, and therefore hysteresis loop [32, 33, 37].

Plotting the hydrogen excess as a function of *W* and *M*, see Fig. S6 of the Supplementary material, confirmed that *M* had no effect on the final texture of the material, as already observed in Fig. 4d). Since Y_{HTC} increases with *M*, higher sucrose concentrations might be used to obtain more AC material and thereby improve the economic balance.

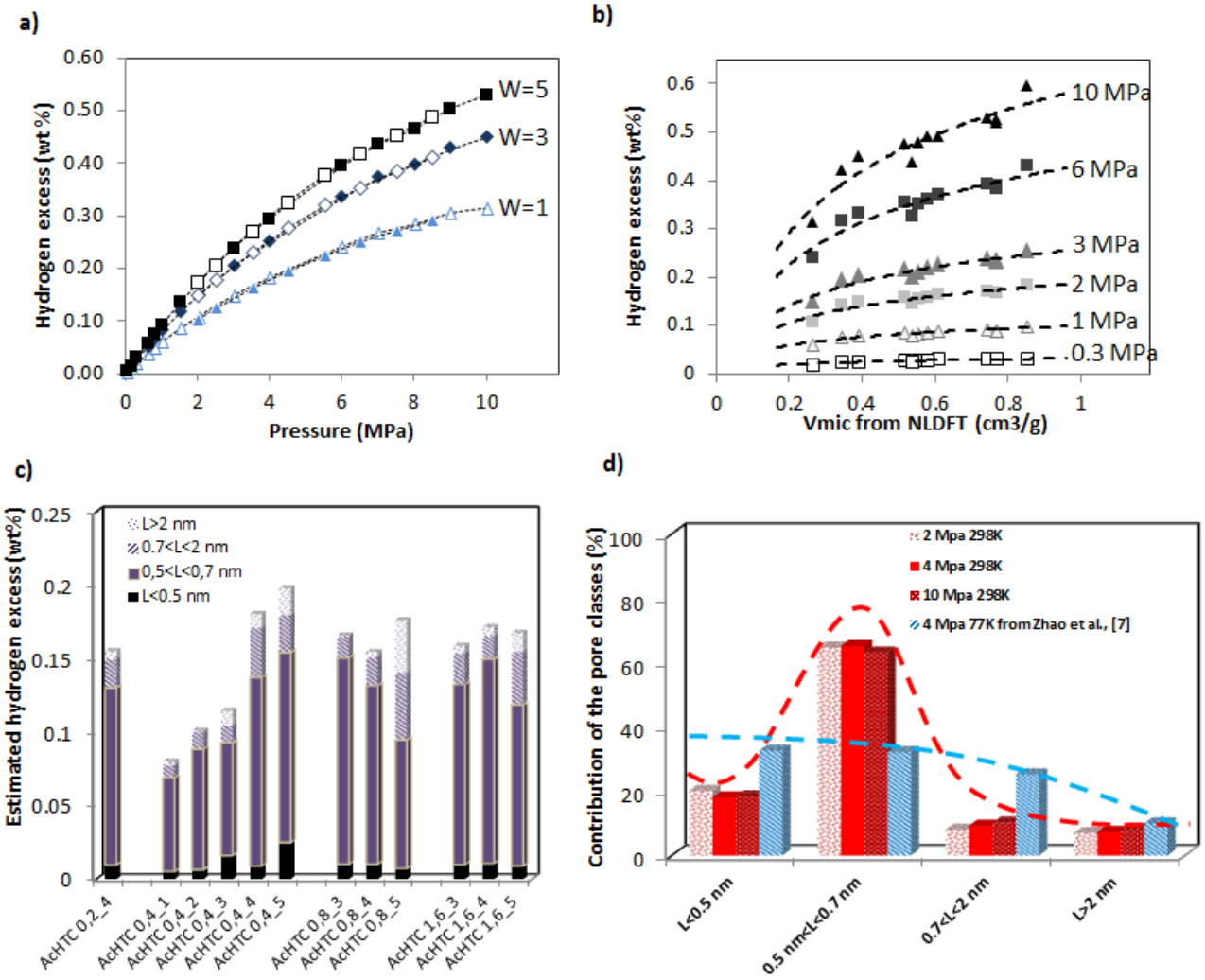

Fig. 6: (a) Excess hydrogen adsorption of the AcHTC_0.4 series for different activation ratios *W*; (b) Correlation between excess hydrogen uptake and micropore volume for different pressures; (c) Contributions of the different kinds of pore volumes to the hydrogen excess uptake at 2 MPa and 298K; (d) Relative contributions of each pore diameter to the hydrogen excess uptake at 2, 4 and 10 MPa at 298K, and at 4 MPa at 77K.

Fig. 6b) shows the dependence of the hydrogen storage capacity on the micropore volume for all the ACs reported in this study at different hydrogen equilibrium pressures, namely: 0.3, 1, 2, 3, 6 and 10 MPa. At low pressure, hydrogen excess poorly depends on the total micropore volume as the hydrogen uptake is low and all ACs have enough micropores to store

this small amount of gas. For higher storage pressures, a linear relationship between hydrogen excess and micropore volume can be observed, as ACs having more micropores are able to store more hydrogen. At the highest pressures, a higher scattering of data points can be observed, probably because hydrogen adsorption not only depends on the micropore volume but also on the PSD. As the total surface area of the ACs is mostly due to microporosity, a similar trend was found when plotting the hydrogen excess as a function of the total surface area.

Cabria et al. [38] theoretically predicted that pores widths should be about 0.6 nm in order to reach the required 3-4% wt.% hydrogen uptake for applications at 300K and at least 10 MPa. In order to calculate the contribution to hydrogen storage of each range of pore widths, we first calculated the contribution to total volume of four ranges of pore widths: < 0.5nm (narrow ultramicropores); 0.5-0.7nm (wider ultramicropores); 0.7-2nm (supermicropores) and 2-50nm (mesopores). We decided to split the ultramicropore range in two subfamilies for studying them separately and for comparing with previous studies on hydrogen storage at 77K [39]. The adsorption data were fitted with the following linear expression:

$$\mathrm{H_2\ excess\ uptake} = \sum_{i=1}^{4} x_i V_i = \sum_{i=1}^{4} H_i \qquad (1)$$

where H_i is the contribution of each width range to the total H_2 excess uptake, and x_i (wt.% g cm^{-3}) and V_i ($cm^3\ g^{-1}$) are weighing coefficient and pore volume of the i^{th} range of pore width, respectively. Applying Eq. (1) with i = 4 to the hydrogen excesses at 2 MPa and 298K of all the ACs presented here, the following polynomial expression was obtained through a multilinear regression:

$$H_{2\,excess}\ (2\ MPa, 298K, wt\%) = 0.173V_1 + 0.556V_2 + 0.070V_3 + 0.060V_4 \qquad (2)$$

The fit to the experimental data was quite good, with a R^2 correlation factor equal to 0.97.

Fig. 6c) represents the hydrogen excess calculated from Eq. (2). The major contribution to hydrogen excess at 298K was due to pores widths between 0.5 nm and 0.7 nm, as predicted by Cabria et al. [38]. This result is different from that obtained by Zhao et al. at 77K and 4 MPa, who concluded that pore widths in the range 0.7-2 nm were the most important for hydrogen storage [39]. Therefore, the same calculations as carried out at 2 MPa were also done at 4 and 10 MPa. Fig. 6d) shows the contribution to hydrogen storage of each range of pore diameter as a function of pressure and temperature. As hydrogen uptake depends on equilibrium pressure and temperature, the contributions to hydrogen storage were expressed as percentages. At 298K, no clear trend was observed when comparing results at different storage pressures, and the small differences between different pressures were attributed to experimental uncertainty. But the major contribution of pores having widths in the 0.5-0.7 nm range was confirmed. As these pores, between 0.5 and 0.7 nm, represent only a minor part of the pore volume, as evidenced in Fig. S7 of the Supplementary material, they are expected to have a high adsorption potential towards hydrogen. At 298K, the most efficient pore class is the one presenting the best balance between volume and width. In addition, as the pressure has no effect on the relative contribution at 298K, the different classes of pores are progressively filled, and none is saturated in the pressure range 0-10 MPa.

The results reported in Fig. 6d) on hydrogen storage at 77 K were taken from Zhao el al. [7] and show that the main contribution to H_2 uptake is due to the narrowest micropores (< 0.5nm). The contribution to hydrogen uptake progressively decreased with increasing pore width. The effect of pore width through the overlap of the adsorption potentials is significantly less important at 77K than at 298K, at which the adsorption potential has to be very high to allow hydrogen adsorption at the carbon surface.

Fig. 7a) shows the dependence of the isosteric heat of adsorption, Q_{st}, on hydrogen uptake (and hence on surface coverage) for four AC's of the AcHTC_0.4_W series, with *W* ranging

from 1 to 4. It can be seen that the AC prepared at W = 1 presented the lowest Q_{st}, whereas ACs prepared at W = 2 and 3 presented similar Q_{st}, around 8 kJ mol^{-1}. The AC prepared at W = 4 had an intermediary Q_{st}, around 7 kJ mol^{-1}. On average, Q_{st} slightly decreased when the coverage increased, this trend was both theoretically and experimentally demonstrated by several authors [40-42].

The values of Q_{st} measured here are somewhat higher than those usually reported for hydrogen on graphite, which is around 4-6 kJ mol^{-1} [40-43]. However, Q_{st} of hydrogen on activated carbons can exceed 6 kJ mol^{-1} [43, 44]. Sevilla et al. [8] also determined Qst values between 6 and 8 kJ mol^{-1} and concluded that it could be due to a high interaction between hydrogen and ACs from hydrothermally carbonized organic materials. In the latter study, hydrochars were also activated by KOH. We think that the high Qst found is more due to the intercalation of potassium ions in the carbon structure, which remain in the activated carbon after washing and induce a stronger physisorption phenomenon, than to an effect of a previous HTC pre-treatment. Enoki et al. [45] studied alkali-metal-graphite intercalation compounds and they concluded that hydrogen was absorbed by physisorption and chemisorption. The activity of the chemisorption increases in the order Cs < Rb < K. Indeed, Contescu et al. [32, 46-49] showed unusually high adsorption heats in KOH activated carbons, attributed to contributions from polarization-enhanced physisorption induced by traces of alkali metals residual from chemical activation.

Fig. 7b) shows the variation of the average Q_{st} and micropore size (L_0) with W for 4 ACs, discontinuous lines are only guides for the eye. L_0 slightly decreased from 0.74 to 0.69nm when W increased from 1 to 2, due to the higher activation and the creation of new pores leading to higher surface area (from 792 to 1014 m^2 g^{-1}, respectively). Further increasing of W produced the widening of micropores, L_0 increased up to 0.70 and 0.88nm at W equal to 3 and 4, respectively. The changes of Q_{st} and L_0 with W were exactly opposite in agreement with

previous experimental and theoretical studies [50, 51]. A maximum of Q_{st} depending on pore size was predicted with Schindler and LeVan [44]. The reason of the small variation of Qst with the quantity adsorbed is due to the fact that the saturation is never reached on the surface of the solid.

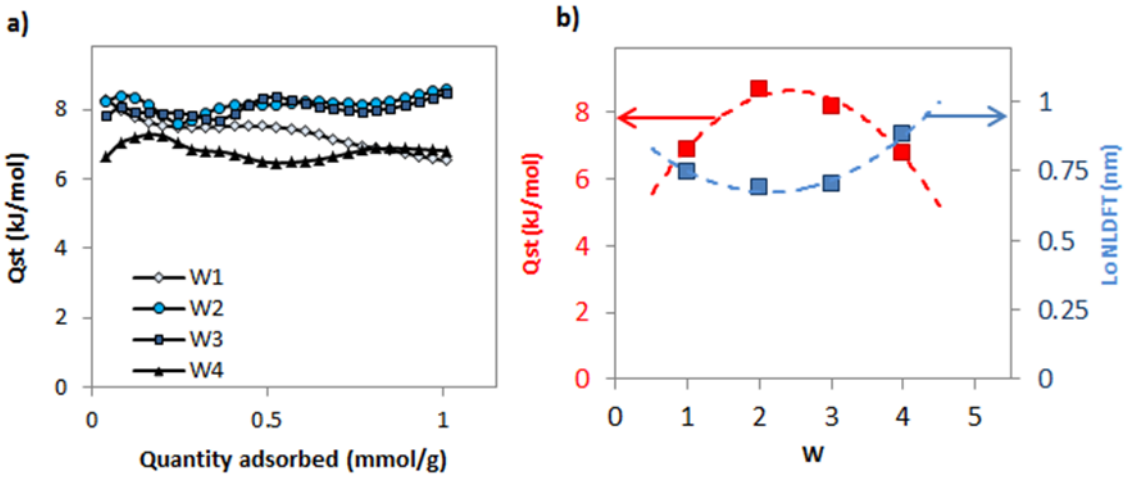

Fig. 7: (a) Isosteric heat of adsorption (Q_{st}) of hydrogen as a function of the amount of adsorbed H_2 and (b) average Q_{st} values for four ACs of the series AcHTC_0.4_W (W = 1, 2, 3 and 4).

Fig. 8 a) shows the direct dependence of isosteric heat of adsorption on pore size. Our results are here compared with theoretical ones for slit pores [44]. As explained before, the values are somewhat higher than the predicted ones; it is probably due to potassium intercalation but also because the pores surface of the solids is not flat like the one used in the theoretical model but corrugated. Nevertheless, the trend can be observed very clearly and the Q_{st} decrease depending while the pore size increases.

Fig. 8 b) shows hydrogen excess at 2 MPa and 298K as a function of micropore volume calculated by the Dubinin-Raduskevich (V_{DR}) method for 38 different ACs. The Dubinin-Raduskevich method is the method mostly used in the literature to calculate the micropore volume [7, 18, 52]. In this figure, we reported results for ACs prepared from silica templates, carbon nanotubes, carbon fibres, subbituminous coal, commercially available carbons and

anthracites [52-54], as well as those obtained in the present study. A linear relationship between hydrogen excess and V_{DR} was observed, whatever the nature of the precursor used. This trend was still valid at 3 MPa (see Fig. S8 of the Supplementary material). Hydrogen storage appears to depend exclusively of the micropore volume. Therefore, we have undoubtedly shown that the interest of a HTC treatment before activation would be more related to the possibility of doping the nanoporous carbon with nanoparticles or heteroatoms in order to improve the hydrogen storage capacity by enhancing hydrogen –surface interactions.

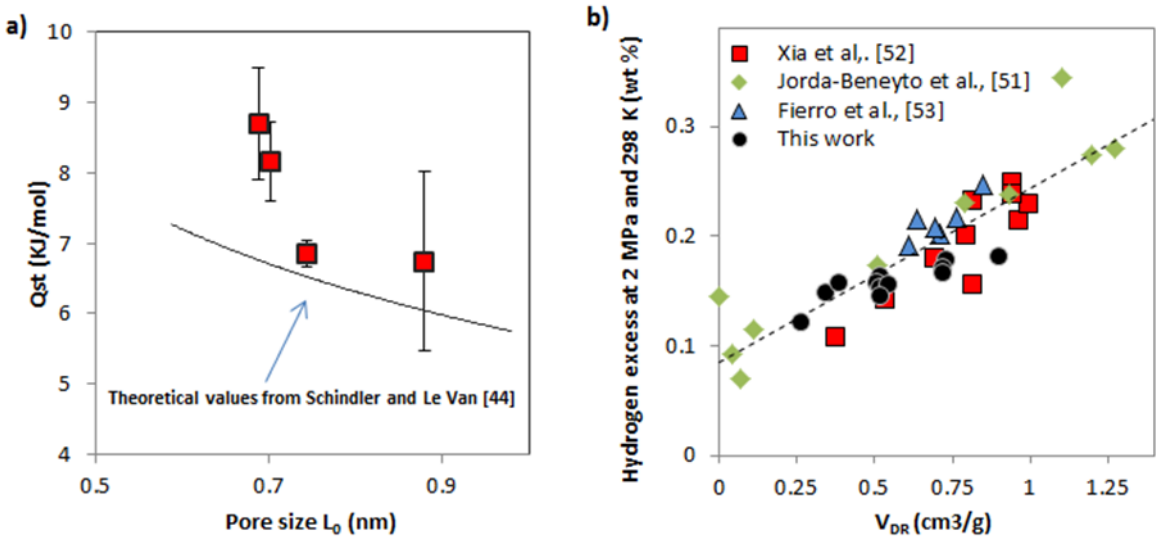

Fig. 8: (a) Comparison between isoteric heat of adsorption from measurement (average values for the AcHTC_0.4_W series) and theoretical values for slit pores from Schindler and Le Van, [44]. (b) Hydrogen excess uptake at 2MPa and 298K as a function of micropore volume for ACs presented in this study and from literature (◆ [53], ■ [52] and ▲ [54]).

4. Conclusions

Activated carbons (ACs) with high apparent surface areas, up to 2703 m^2/g, were obtained by KOH activation of hydrothermally treated sucrose. Different sucrose concentrations and activating ratios, W, were used. The main factor affecting the pore texture of ACs was *W*. Increasing the initial concentration of the sucrose solution increased the hydrochar yield whereas the activation yield only depended on *W*. Therefore, high concentrations of sucrose should be preferably submitted to HTC to increase the total yield of the process. Hydrothermal carbonisation allowed increasing considerably carbon yield when compared to direct activation of sucrose by KOH but little differences were found when compared to KOH activation of prepyrolysed sucrose.

A maximum hydrogen excess adsorption of 0.59 wt% was obtained in agreement with values reported in the open literature for ACs having similar micropore volumes. Excess hydrogen uptake depends linearly on the micropore volume. We proved that pores having widths ranging from 0.5 to 0.7 nm are the most relevant to store hydrogen at 298 K independently of the pressure. High isosteric heat of adsorptions, Q_{st}, around 7-8 kJ mol^{-1} were determined, probably due to KOH intercalation in the carbon structure. Q_{st} depended on the average micropore size and a maximum was found for a L_0 equal to 0.7nm.

We undoubtedly showed that pre-treating sucrose by HTC before KOH activation does not provide any beneficial effect on hydrogen storage when compared to KOH activation of pyrolysed sucrose. However, as HTC constitutes a good method to incorporate transition metals and heteroatoms into the carbon structure, the present work is expected to be a reference for further studies on carbon doping in hydrothermal conditions, which are presently in progress.

Acknowledgements

The authors gratefully acknowledge the financial support of the CPER 2007-2013 “Structuration du Pôle de Compétitivité Fibres Grand’Est” (Competitiveness Fibre Cluster), through local (Conseil Général des Vosges), regional (Région Lorraine), national (DRRT and FNADT) and European (FEDER) funds. Part of this work was supported by CHEERS project (FEDER funds) and the COST Action MP1103 “Nanostructured materials for solid-state hydrogen storage”. We thank Mr. P. Gadonneix and Dr. A. Szczurek for carrying out SEM and elemental analysis.

References

[1] B. Stefano, C. Massimo, G. Romano, P. Davide, Storage applications for Smartgrids, Electric Power Systems Research, 2014, pp. 109-117.

[2] C. Darras, M. Muselli, P. Poggi, C. Voyant, J.C. Hoguet, F. Montignac, PV output power fluctuations smoothing: The MYRTE platform experience, International Journal of Hydrogen Energy 37(19) (2012) 14015-14025.

[3] T. O'Garra, S. Mourato, P. Pearson, Investigating attitudes to hydrogen refuelling facilities and the social cost to local residents, Energy Policy 36(6) (2008) 2074-2085.

[4] F. Sherry-Brennan, H. Devine-Wright, P. Devine-Wright, Public understanding of hydrogen energy: A theoretical approach, Energy Policy 38(10) (2010) 5311-5319.

[5] L. Schlapbach, A. Zuttel, Hydrogen-storage materials for mobile applications, Nature 414(6861) (2001) 353-358.

[6] V. Fierro, A. Szczurek, C. Zlotea, J.F. Mareche, M.T. Izquierdo, A. Albiniak, M. Latroche, G. Furdin, A. Celzard, Experimental evidence of an upper limit for hydrogen storage at 77 K on activated carbons, Carbon 48(7) (2010) 1902-1911.

[7] W. Zhao, V. Fierro, C. Zlotea, E. Aylon, M.T. Izquierdo, M. Latroche, A. Celzard, Optimization of activated carbons for hydrogen storage, International Journal of Hydrogen Energy 36(18) (2011) 11746-11751.

[8] W. Zhao, V. Fierro, N. Fernandez-Huerta, M.T. Izquierdo, A. Celzard, Impact of synthesis conditions of KOH activated carbons on their hydrogen storage capacities, International Journal of Hydrogen Energy 37(19) (2012) 14278-14284.

[9] D.J. Durbin, C. Malardier-Jugroot, Review of hydrogen storage techniques for on board vehicle applications, International Journal of Hydrogen Energy 38(34) (2013) 14595-14617.

[10] M. Sevilla, A.B. Fuertes, R. Mokaya, High density hydrogen storage in superactivated carbons from hydrothermally carbonized renewable organic materials, Energy & Environmental Science 4(4) (2011) 1400-1410.

[11] M. Sevilla, A.B. Fuertes, Chemical and Structural Properties of Carbonaceous Products Obtained by Hydrothermal Carbonization of Saccharides, Chemistry-a European Journal 15(16) (2009) 4195-4203.

[12] F. Bergius, Die Anwendung von hohen Drucken bei chemischen und chemisch-technischen Vorgängen, Zeitschrift für Elektrochemie, 1913, p. 661.

[13] A.N. Stranges, Bergius Friedrich and the transformation of coal-liquefaction from empiricism to a science-based technology, Journal of Chemical Education 65(9) (1988) 749-751.

[14] C.Y. Chen, X.D. Sun, X.C. Jiang, D. Niu, A.B. Yu, Z.G. Liu, J.G. Li, A Two-Step Hydrothermal Synthesis Approach to Monodispersed Colloidal Carbon Spheres, Nanoscale Research Letters 4(9) (2009) 971-976.

[15] M.M. Titirici, R.J. White, C. Falco, M. Sevilla, Black perspectives for a green future: hydrothermal carbons for environment protection and energy storage, Energy & Environmental Science 5(5) (2012) 6796-6822.

[16] F.L. Braghiroli, V. Fierro, M.T. Izquierdo, J. Parmentier, A. Pizzi, A. Celzard, Kinetics of the hydrothermal treatment of tannin for producing carbonaceous microspheres, Bioresource Technology 151 (2014) 271-277.

[17] M. Sevilla, A.B. Fuertes, The production of carbon materials by hydrothermal carbonization of cellulose, Carbon 47(9) (2009) 2281-2289.

[18] A.J. Romero-Anaya, M. Ouzzine, M.A. Lillo-Rodenas, A. Linares-Solano, Spherical carbons: Synthesis, characterization and activation processes, Carbon 68 (2014) 296-307.

[19] X.Q. Fan, L.X. Zhang, G.B. Zhang, Z. Shu, J.L. Shi, Chitosan derived nitrogen-doped microporous carbons for high performance CO2 capture, Carbon 61 (2013) 423-430.

[20] L. Zhao, N. Baccile, S. Gross, Y. Zhang, W. Wei, Y. Sun, M. Antonietti, M.-M. Titirici, Sustainable nitrogen-doped carbonaceous materials from biomass derivatives, Carbon 48(13) (2010) 3778-3787.

[21] F.L. Braghiroli, V. Fierro, M.T. Izquierdo, J. Parmentier, A. Pizzi, A. Celzard, Nitrogen-doped carbon materials produced from hydrothermally treated tannin, Carbon 50(15) (2012) 5411-5420.

[22] M. Li, W. Li, S.X. Liu, Hydrothermal synthesis, characterization, and KOH activation of carbon spheres from glucose, Carbohydrate Research 346(8) (2011) 999-1004.

[23] M. Sevilla, A.B. Fuertes, Sustainable porous carbons with a superior performance for CO2 capture, Energy & Environmental Science 4(5) (2011) 1765-1771.

[24] F. Cheng, J. Liang, J. Zhao, Z. Tao, J. Chen, Biomass waste-derived microporous carbons with controlled texture and enhanced hydrogen uptake, Chemistry of Materials 20(5) (2008) 1889-1895.

[25] F. Stoeckli, A. Slasli, D. Hugi-Cleary, A. Guillot, The characterization of microporosity in carbons with molecular sieve effects, Microporous and Mesoporous Materials 51(3) (2002) 197-202.

[26] J. Jagiello, J.P. Olivier, 2D-NLDFT adsorption models for carbon slit-shaped pores with surface energetical heterogeneity and geometrical corrugation, Carbon 55 (2013) 70-80.

[27] A. Szczurek, G. Amaral-Labat, V. Fierro, A. Pizzi, A. Celzard, Chemical activation of tannin-based hydrogels by soaking in KOH and NaOH solutions, Microporous and Mesoporous Materials 196 (2014) 8-17.

[28] Van Krevelen, D. W., Development of coal research-A review, Fuel, 1982, pp. 786-790.

[29] J. Alacaniz-Monge, M.J. Illan-Gomez, Insight into hydroxides-activated coals: Chemical or physical activation, Journal of Colloid and Interface Science 318(1) (2008) 35-41.

[30] V. Fierro, G. Muniz, A.H. Basta, H. El-Saied, A. Celzard, Rice straw as precursor of activated carbons: Activation with ortho-phosphoric acid, Journal of Hazardous Materials 181(1-3) (2010) 27-34.

[31] M.A. Lillo-Rodenas, J.P. Marco-Lozar, D. Cazorla-Amoros, A. Linares-Solano, Activated carbons prepared by pyrolysis of mixtures of carbon precursor/alkaline hydroxide, Journal of Analytical and Applied Pyrolysis 80(1) (2007) 166-174.

[32] V.V. Bhat, C.I. Contescu, N.C. Gallego, F.S. Baker, Atypical hydrogen uptake on chemically-activated, ultramicroporous carbon, Carbon 48(5) (2010) 1331-1340.

[33] V.V. Bhat, C.I. Contescu, N.C. Gallego, Kinetic effect of Pd additions on the hydrogen uptake of chemically-activated ultramicroporous carbon, Carbon 48(8) (2010) 2361-2364.

[34] E. Poirier, A. Dailly, Investigation of the hydrogen state in IRMOF-1 from measurements and modeling of adsorption isotherms at high gas densities, Journal of Physical Chemistry C 112(33) (2008) 13047-13052.

[35] J. Moellmer, A. Moeller, F. Dreisbach, R. Glaeser, R. Staudt, High pressure adsorption of hydrogen, nitrogen, carbon dioxide and methane on the metal-organic framework HKUST-1, Microporous and Mesoporous Materials 138(1-3) (2011) 140-148.

[36] W.B. Leung, N.H. March, Primitive phase diagram for hydrogen, Physics Letters, 1976, p. 425-426.

[37] C.I. Contescu, D. Saha, N.C. Gallego, E. Mamontov, A.I. Kolesnikov, V.V. Bhat, Restricted dynamics of molecular hydrogen confined in activated carbon nanopores, Carbon 50(3) (2012) 1071-1082.

[38] I. Cabria, M.J. Lopez, J.A. Alonso, The optimum average nanopore size for hydrogen storage in carbon nanoporous materials, Carbon 45(13) (2007) 2649-2658.

[39] W. Zhao, V. Fierro, C. Zlotea, E. Aylon, M.T. Izquierdo, M. Latroche, A. Celzard, Activated carbons with appropriate micropore size distribution for hydrogen adsorption, International Journal of Hydrogen Energy 36(9) (2011) 5431-5434.

[40] E. Dundar, R. Zacharia, R. Chahine, P. Benard, Modified potential theory for modeling supercritical gas adsorption, International Journal of Hydrogen Energy 37(11) (2012) 9137-9147.

[41] Q. Zheng, X. Wang, S. Gao, Adsorption equilibrium of hydrogen on graphene sheets and activated carbon, Cryogenics 61 (2014) 143-148.

[42] K. Vasanth Kumar, M.C. Monteiro de Castro, M. Martinez-Escandell, M. Molina-Sabio, F. Rodriguez-Reinoso, Heat of adsorption and binding affinity for hydrogen on pitch-based activated carbons, Chemical Engineering Journal 168(2) (2011) 972-978.

[43] A. Gigras, S.K. Bhatia, A.V.A. Kumar, A.L. Myers, Feasibility of tailoring for high isosteric heat to improve effectiveness of hydrogen storage in carbons, Carbon 45(5) (2007) 1043-1050.

[44] B.J. Schindler, M.D. LeVan, The theoretical maximum isosteric heat of adsorption in the Henry's law region for slit-shaped carbon nanopores, Carbon 46(4) (2008) 644-648.

[45] T. Enoki, S. Miyajima, M. Sano, H. Inokuchi, Hydrogen alkali-metal graphite ternary intercalation compounds, Journal of Materials Research 5(2) (1990) 435-466.

[46] L. Duclaux, S. Los, P. Azais, R. Pellenq, Y. Breton, O. Isnard, Deuterium adsorption in carbon single walled carbon nanotubes doped by lithium and potassium: Adsorption isotherms and in situ neutron diffraction, Journal of Physics and Chemistry of Solids 67(5-6) (2006) 1122-1126.

[47] H. Zhang, V.V. Bhat, P.X. Feng, C.I. Contescu, N.C. Gallego, Effect of potassium-doping on the microstructure development in polyfurfuryl alcohol - derived activated carbon, Carbon 50(14) (2012) 5278-5285.

[48] C. Contescu, N. Gallego, V. Bhat, Effect of metal additions on the hydrogen uptake of microporous carbon at near-ambient temperature, Conference: Carbon 2010, the Annual World Conference on Carbon, Clemson, SC, USA, 20100711, 20100716, 2010.

[49] R.J.M. Pellenq, F. Marinelli, J.D. Fuhr, F. Fernandez-Alonso, K. Refson, Strong physisorption site for H-2 in K- and Li-doped porous carbons, Journal of Chemical Physics 129(22) (2008).

[50] Y.F. He, N.A. Seaton, Monte Carlo simulation and pore-size distribution analysis of the isosteric heat of adsorption of methane in activated carbon, Langmuir 21(18) (2005) 8297-8301.

[51] S.H. Jhung, H.K. Kim, J.W. Yoon, J.S. Chang, Low-temperature adsorption of hydrogen on nanoporous aluminophosphates: Effect of pore size, Journal of Physical Chemistry B 110(19) (2006) 9371-9374.

[52] M. Jorda-Beneyto, F. Suarez-Garcia, D. Lozano-Castello, D. Cazorla-Amoros, A. Linares-Solano, Hydrogen storage on chemically activated carbons and carbon nanomaterials at high pressures, Carbon 45(2) (2007) 293-303.

[53] K. Xia, J. Hu, J. Jiang, Enhanced room-temperature hydrogen storage in super-activated carbons: The role of porosity development by activation, Applied Surface Science 315 (2014) 261-267.

[54] V. Fierro, W. Zhao, M.T. Izquierdo, E. Aylon, A. Celzard, Adsorption and compression contributions to hydrogen storage in activated anthracites, International Journal of Hydrogen Energy 35(17) (2010) 9038-9045.